$LaPO_4$:Er micro-spheres with high NIR luminescent quantum yield

J. García-Sevillano[1], N. O. Núñez[2], E. Cantelar[1], A. Justo[2], M. Ocaña[2] and F. Cussó[1]

[1]Departamento de Física de Materiales, C-04, Facultad de Ciencias, Universidad Autónoma de Madrid, Avda. Francisco Tomás y Valiente, 7. 28049 - Madrid (Spain).

[2]Instituto de Ciencia de Materiales de Sevilla, CSIC-US, c/ Américo Vespucio 49, Isla de la Cartuja. 41092 - Sevilla (Spain).

ABSTRACT

Er-doped $LaPO_4$ micro-spheres have been synthesized by spray pyrolysis and the near infrared (NIR) properties have been characterized. It has been found that, following an adequate post-annealing treatment, the emission properties are remarkably improved. The NIR luminescence intensity is highly enhanced and its decay time increases to a value almost coincident with the reported radiative lifetime, which implies that the quantum yield approaches $\eta \approx 100\%$. This improvement in luminescence characteristics is probably related to the suppression of residual OH^- radicals, that otherwise act as NIR luminescence quenchers, and to the increase in material's crystallinity.

1.- INTRODUCTION

Lanthanide phosphate ($LaPO_4$) and, in particular, its monoclinic polymorph (monazite), has been widely used as a host for the preparation of lanthanide- based phosphors. In fact, doped with Ce and Tb constitutes one of the classical phosphors used in high-quality fluorescent lighting due to its high quantum yield and stability at high temperature [1-4]. By varying the dopants (Pr, Nd, Eu, …) the optical properties can be tuned over a wide spectral range, with emerging applications in different fields such as biomedicine [5-6], photonic band gap materials or optical amplification [7-8]. In particular, for optical amplifiers and lasers, Er becomes the most interesting dopant because of its characteristic emission, at around 1.5 μm, coincident with the transparency window of optical fibers [8-9]. Along this line, there has been a considerable effort along the last years in order to prepare Er doped phosphate particles incorporated into polymer-based components, in order to improve luminescence characteristics and trying to achieve long lifetimes and high quantum efficiencies [10-17]. The data reported in the literature for the 1.5 μm emission lifetime vary within a very large range (60 μs [14] to 3.7 ms [17]), reflecting possibly the large variety of dopants concentration, particle size and fabrication processes; affecting material's properties such as crystallinity or impurities content [10-17].

Spray pyrolysis is a well known technique for the synthesis of powdered materials, whose main advantages are simplicity and continuous character, which, along with its suitability to control particle size (micrometric) and shape (spherical), make it very attractive for industrial purposes [18-19]. Recently, this method has been used to prepare $LaPO_4$ spheres doped with Ce and Tb ions, which showed a high luminescence efficiency after a post heating treatment at >1300ºC [20-21]. However, up to our knowledge, this synthesis method has never been applied to the synthesis of Er-doped $LaPO_4$ with NIR luminescence.

In the present work we explore the applicability of the spray pyrolysis procedure for the synthesis of Er-doped $LaPO_4$ powders with improved NIR luminescent characteristics. It is found that it is possible to prepare $LaPO_4$:Er micro-spheres with good IR emission characteristics, including a relatively long lifetime. Following an adequate post-annealing treatment, the emission properties are remarkably enhanced, with its decay time increasing to a value almost coincident with the reported radiative lifetime, which implies that the NIR luminescent quantum yield (QY) approaches $\eta \approx 100\%$. We also show that the improvement in luminescence QY is probably related to the suppression of residual OH radicals, that otherwise act as efficient NIR luminescence quenchers, and to a parallel crystallinity increase.

2.- EXPERIMENTAL

2.1.- Synthesis of samples

Erbium-doped lanthanum phosphate with nominal composition $Er_{0.02}La_{0.98}PO_4$ was prepared by pyrolysis of a liquid aerosol generated from an acidic (0.3 mol dm^{-3} HCl) solution 0.049 mol dm^{-3} in lanthanum nitrate ($La(NO_3)_3 \cdot 6H_2O$, Fluka, 99%), 0.001 mol dm^{-3} in europium chloride ($ErCl_3 \cdot 6H_2O$, Aldrich, 99.9%) and 0.05 mol dm^{-3} in H_3PO_4. This solution was sprayed into an expansion chamber using a glass nozzle and air at constant pressure (0.5 kg cm^{-2}) as a carrier gas and the resulting aerosol was introduced into two consecutive furnaces kept at 250 and 600ºC, respectively, in which the liquid droplets were first dried and then, thermally decomposed. The so obtained solid particles were collected on a glass filter with a very high efficiency. A more detailed description of the experimental setup can be found in reference [18].

The obtained powdered samples were calcined at different temperatures (up to 950 ºC) for 4 h, using a heating rate of 10 ºC min^{-1}.

2.2.- Characterization techniques

The morphology of the particles was examined by scanning electron microscopy (SEM-FEG) (Model S4800, Hitachi).

The quantitative composition of the samples (Er/La mol ratio) was determined by the ICP technique (Model Ultima 2, Horiba Jobin Yvon).

The Fourier transform infrared spectra (FTIR) were recorded in a Jasco FT/IR-6200 Fourier transform spectrometer. For this purpose, the samples were diluted in KBr pellets. Thermogravimetric analyses (TGA) were performed (Q600 TA Instrument) in air atmosphere using a heating rate of 10 °C min^{-1}.

The crystalline phases present in the samples were identified by X-ray diffraction (XRD) (Model X´Pert Pro, Panalytical). Unit cell parameters of the sample calcined at 950 ºC were determined by Rietveld refinement, using the X´Pert HighScore Plus software, from the XRD data collected at intervals of 0.02° (2θ) for an accumulation time for interval of 10 s. The crystallographic data for the $LaPO_4$ structure were taken from reference [22].

Crystallite size was evaluated according to the Scherrer formula from the (2 0 0) XRD reflection at 2θ ~ 26.8º or from the SEM pictures taken at high magnification.

Optical absorption spectra in the UV-Visible and near infrared range were measured by using a Perkin Elmer Lambda 1050 spectrophotometer. For that purpose the particles were mounted in a specially designed holder, constructed by using a 100 μm thick spacer, with a 10 mm × 5 mm rectangular opening, sandwiched by two microscope slide covers. The $LaPO_4$:Er powders were included filling the cavity.

Luminescence was obtained either under CW or pulsed excitation, at different wavelengths, using several sources. For CW measurements either an Ar^+ laser (Spectra Physics, model 2040E), Ti: Sapphire laser (Spectra Physics, model 3900) or a diode laser (LIMO FQ-A 0063) have been used. The luminescent signal was dispersed by using a

Princeton Instrument monochromator (ARC SpectraPro 500-i model) and detected with a Judson InGaAs photodiode (G 5883). For lifetime measurements, excitation was performed by using the diode laser, in pulsed configuration, and the transient luminescence was averaged and recorded with a digital Tektronix TDS 420 oscilloscope.

3.- RESULTS AND DISCUSSION

3.1.- Structural characterization

The Er content (Er/Er+La mol ratio) of the synthesized $Er_{0.02}La_{0.98}PO_4$ sample experimentally determined (1.95%) was in agreement with the nominal value (2%). An illustrative SEM picture of this sample (as prepared) is shown in the upper part of Figure 1, which shows that it consisted of spherical particles of broad size distribution (< 10 μm). The XRD pattern obtained for these spheres (Fig. 2, lower curve) was consistent with monoclinic $LaPO_4$ [JCPDS file 1-83-651] with low crystallinity as revealed by the broadening of the XRD reflections. In fact, the crystallite size, estimated for this sample by using the Scherrer formula, was much smaller (12 nm) (Table 1) than the size of the spheres (Fig. 1), manifesting their polycrystalline character. The FTIR spectrum of this sample displayed bands at >1200 cm^{-1} mainly due to the lattice vibrations [23], along with a much less intense absorption at 1380 cm^{-1} corresponding to the unreacted nitrate anions and two broad bands at 1630 and 3390 attributed to adsorbed water [24] (Fig. 3). Nevertheless, the possible contribution to the latter band of OH^- anions of different origin cannot be neglected. The TGA curve recorded for this sample presented a weight loss of 6 % in the 25-800 ºC range (Fig. 4). Such a weight loss must be ascribed to the release of such impurities as suggested by FTIR spectroscopy (Fig. 3). Thus, the nitrate disappeared in the spectrum of the sample heated at 600ºC, whereas the intensity of the water bands weakened and completely disappeared at 800ºC. No further changes were observed on further heating at higher temperatures up to 950 ºC. The thermal treatment also gave rise to a sharpening of the XRD peaks (Fig. 2) indicating an increase of sample

crystallinity, accompanied by a change in the microstructure of the spheres, as illustrated in Fig.1 for the sample heated at 950 ºC, in which the spheres appeared clearly composed by much smaller aggregated crystallites. The size of such crystallites was found to progressively increased from 12 nm, for the as prepared sample to 50-150 nm, after heating at 950 ºC (Table 1).

The incorporation of Er^{3+} to the $LaPO_4$ structure was confirmed by the unit cell parameters obtained for the sample calcined at 950 ºC, which were lower than those corresponding to an undoped sample (Table 2), in agreement with the smaller size of the Er^{3+} cation in the ninefold coordination present in the monoclinic structure (1.062 Å,) when compared with that of La^{3+} (1.216 Å) [25]

3.2.- Optical characterization

Figure 5 shows the room temperature absorption spectra of the $LaPO_4$:Er^{3+} powders. The absorption bands of Er^{3+} ions are clearly visible, and identified in the figure with the labels of the corresponding excited multiplets.

Figure 6 shows the near-infrared (NIR) luminescence spectra of Er^{3+} in $LaPO_4$, under NIR excitation, using a Ti: Sapphire laser at $\lambda_{exc} \approx 800$ nm, corresponding to the $^4I_{15/2} \rightarrow {}^4I_{9/2}$ transition, as indicated in the inset. It basically consists on a single broad emission, extending from 1.45 μm to 1.65 μm, which corresponds to the $^4I_{13/2} \rightarrow {}^4I_{15/2}$ transition, although a careful inspection of spectra allows also identifying a very weak emission at around 980 nm, corresponding to the $^4I_{11/2} \rightarrow {}^4I_{15/2}$ transition. The emission is coincident to that obtained after excitation to other multiplets, either the $^4I_{11/2}$ multiplet using a diode laser operating at $\lambda_{exc} \approx$ 980 nm, or to the upper $^4F_{7/2}$ multiplet using an Ar^+ laser at $\lambda_{exc} \approx 488$ nm, in accordance with the results previously reported by other researchers [11]. This confirms that $LaPO_4$: Er is an excellent NIR emitting material that can be efficiently pumped to different Er-multiplets, from where a non-radiative cascade ultimately populates the $^4I_{13/2}$ multiplet, from where the 1.5 μm

emission occurs, as indicated in the inset. This characteristic is one of the recognized advantages of phosphate materials to be used for optical lasers and amplifiers [8-9].

Nevertheless, the luminescence intensity of our particles is dependent of the thermal treatment given to the samples. As prepared material displays a relatively low luminescent intensity, which is substantially increased by calcination. In figure 6 the IR luminescence of samples annealed at different temperatures is represented and it is apparent that the luminescence is strongly increased when compared to as prepared powders.

This is not surprising considering that the FTIR spectrum of these samples revealed the presence of some unreacted components (see Figure 3) that may act as luminescence quenchers. Particularly relevant is the presence of OH^- groups, that can be present in different forms and that are known to be efficient quenchers of the 1.5 μm emission of Er^{3+} ions [11-13, 26-30]. As it has been indicated above, TGA data reveal a weight loss when the powders are calcined in the 25 - 800 ºC range (Fig. 4), that can be correlated to the disappearance of water (and nitrate) bands in the FTIR spectrum of the heated samples. Further heating above 1000 ºC did not produce additional weight losses. Similar effects have been observed in Nd-doped $LaPO_4$ where it has been demonstrated that calcination and impurity suppression are directly associated to an increase in the luminescence efficiency [31].

In order to explore more quantitatively whether the suppression of these impurities is associated to an increase of the NIR luminescence quantum yield of the $LaPO_4$:Er powders, the dependence of the fluoresecence decay time of the 1.5 μm emission ($^4I_{13/2} \rightarrow {}^4I_{15/2}$ transition) for samples subjected to different calcination temperatures, has been investigated. The results are presented in Figure 7, where the luminescence decay after pulsed laser excitation is presented. It can be clearly observed that the NIR luminescence lifetime increases as the temperature of calcination is raised.

The luminescence decays are not single exponentials but they can be conveniently described by using a double exponential decay, as it has been observed in many other powdered materials [32-36]:

$$I(t)/I_0 = A_S \exp(-t/\tau_{short}) + A_L \exp(-t/\tau_{long}) \quad (1)$$

The calculated decays are represented by the continuous lines in figure 7 and the corresponding fitting parameters are summarized in Table 3, together with the average decay time, defined as:

$$\langle \tau \rangle = \frac{\int_0^\infty tI(t)dt}{\int_0^\infty I(t)dt} = \frac{A_1\tau_1^2 + A_2\tau_2^2}{A_1\tau_1 + A_2\tau_2} \quad (2)$$

From the data collected in Table 3, it can be observed that while pristine material has a relatively short average lifetime (around 0.76 ms) it is lengthened with calcination, reaching a value $<\tau> \approx 6.47$ ms when calcined at 950 ºC. This last value is very close to the reported radiative lifetime ($\tau_{rad} \approx 6.71$ ms) [17]. The relative weight of the fast and slow components varies also with calcination temperature. While the fast component represents almost a 40% of the emission, its intensity is reduced as the calcination temperature increases, and the longest component becomes dominant, reaching an 80% of the emission for the samples calcined at 950 ºC.

This increase in the NIR luminescence decay time can also be expressed in terms of the luminescence quantum yield (η) that can be calculated as:

$$\eta = \frac{A_{rad}}{A_{Total}} = \frac{A_{rad}}{A_{rad} + A_{no-rad}} = \frac{\tau_{exp}}{\tau_{rad}} \quad (3)$$

where $A_{rad} = 1/\tau_{rad}$ represents the radiative transition rate and is equal to the reciprocal radiative lifetime, whereas $A_{total} = A_{rad} + A_{no\text{-}rad} = 1/\tau_{exp}$ represents the total transition rate which includes radiative plus all possible non-radiative channels such as multiphonon relaxation or energy transfer to luminescence quenchers. The total de-excitation rate, in the case of a single exponential decay, is the reciprocal of the measured lifetime (τ_{exp}). In our case, where the decay is multicomponent, we have taken the reciprocal of the average decay time (eq. (2)) as a representative figure to represent the average transition rate and luminescent quantum yield. Its value is incorporated in the last column of Table 3 and represented in Figure 8 vs. calcination temperature. It can be observed that as prepared material has a modest (11 %) luminescent quantum yield, which increases monotonously with calcination temperature, reaching values substantially higher and even approaching the theoretical limit of 100 % when calcination is performed above 900 ºC.

In fact, this possibility is not surprising, considering that in other materials, the luminescence quantum efficiency of the $^4I_{13/2}$ Er^{3+} level approaches such theoretical 100 % limit [37-43]. The non-radiative component of the decay includes, in general, intrinsic multiphonon de-excitation of the $^4I_{13/2}$ multiplet plus other extrinsic de-excitation channels, which include impurities quenching that is particularly relevant in nano- and submicrometer sized materials. If these additional extrinsic channels are suppressed, the only non-radiative channel remaining is the intrinsic multiphonon component. And this rate decreases exponentially with the number of phonons needed to bridge the gap between the emitting and the lower lying level [44-49].

For the 1.5 μm emission of Er^{3+}, the gap between the emitting $^4I_{13/2}$ multiplet and the lower lying $^4I_{15/2}$ ground state is sufficiently high ($\Delta E \approx 6500$ cm^{-1}) to preclude efficient non-

radiative de-excitation. We can make an estimation of the multiphonon decay rate considering that it can be expressed as :

$$A_{no-rad} = \beta \exp[-\alpha(\Delta E - 2\hbar\Omega)] \quad (4)$$

where ΔE is the energy gap, $\hbar\Omega$ is the phonon energy of the host material and α and β are parameters characteristic of the material. The host dependence of the non-radiative decay rate is basically governed by its phonon energy, while the parameters α and β are relatively insensitive to the host [48,49].

We may therefore make a reasonable estimation by using the parameters reported for phosphate glasses ($\alpha \approx 4{,}7 \times 10^{-3}$ cm, $\beta \approx 6{,}2 \times 10^{7}$ s^{-1} [48]) , and it is obtained that even in the high phonon energy material that is $LaPO_4$ ($\hbar\Omega \approx 1100$ cm^{-1} [50]), the calculated multiphonon transition rate is: $A_{no\text{-}rad} \approx 0.1$ s^{-1}, which is much smaller that the reported radiative rate ($A_{rad} \approx 149$ s^{-1} (= 1/6.71 ms)) and hence a luminescence quantum efficiency close to 100% would be expected, provided that extrinsic quenching factors would be efficiently suppressed.

At this point we should consider that it is generally accepted the detrimental effect of impuritites on the luminescence efficiency, acting as quenchers. Particularly OH^- radicals are known to be efficient Er^{3+}-luminescence quenchers [29-31, 51-56], because of its vibration energy and that only 2 phonons are needed to match the energy gap of the 1.5 μm emission. In fact, it has been demostrated in phosphate glasses that there is a direct releationship between OH^- content and the reduction of the observed luminescence lifetime [55].

As we have indicated above in relation to the FTIR spectra and TGA curves (Figures 3 & 4), the $LaPO_4$:Er microspheres synthesized in the present work incorporate some OH^- (and nitrate) radicals, which are efficiently suppressed upon calcination at 800ºC. A similar result has been also reported, for Nd-doped LaPO4 [31]. Therefore, our luminescence results are

perfectly compatible with the above mentioned arguments and the fact that in $LaPO_4$ it is possible to remove very efficiently remaining impurities by calcination. Nevertheless, we cannot exclude the possibility that other factors accompanying the calcination process could also contribute to the enhancement of the luminescence quantum efficiency. In particular, the fact that the crystallinity of the samples is also improved by calcination (see figure 3 and Table 1) may also have some incidence in the observed improvement.

We may therefore conclude that it is possible to synthesized Er-doped $LaPO_4$ submicron-sized spheres that, upon a simple calcination process at 950 ºC, are effectively released of undesirable luminescence quenchers and, simultaneously, the crystallinity is improved, which allows to reach a very high luminescence quantum yield (96 %) in the NIR.

Ackn**owledgements**

This work was partially supported by Ministerio de Ciencia e Innovación and Comunidad de Madrid under projects CRONOSOMATS (MAT2009-14102) and MICROSERES-CM (P2009/TIC-1476). Also, it was supported by Junta de Andalucía (Grant FQM6090).

REFERENCES

[1] W. van Schaik, S. Lizzo, W. Smith, G. Blasse, J. Electrochem. Soc. 140 (1993) 216-222.

[2] Y.C. Kang, E.J. Kim, D.Y. Lee, H.D. Park, J. Alloys Compd. 347 (2002) 266-270.

[3] R.P. Rao, D.J. Devine, J. Lumin. 87-89 (2000) 1260-1263.

[4] N.O. Nuñez, S.R. Liviano, M. Ocaña, J. Colloid Interface Sci. 349 (2010) 484-491.

[5] F. Meiser, C. Cortez, F. Caruso, Angew. Chem., Int. Ed. 43 (2004) 5954-5957.

[6] J. Woodward, S.J. Kennel, A. Stuckey, D. Osborne, J. Wall, A.J. Rondinone, R.F. Standaert, S. Mirzadeh, Bioconjugate Chem. 22 (2011) 766-776.

[7] A. Oertel, C. Lengler, T. Walther, M. Haase, Chem. Mater. 21 (2009) 3883-3888.

[8] D.B. Jonathan, M. Pollnau, Laser & Photon. Rev. 5 (2011) 368-403.

[9] E. Cantelar, D. Jaque, G. Lifante, Opt. Mater. 34 (2012) 555-571.

[10] D.N. Reinhoudt, C.J.M. van Veggel, Adv. Mater. 14 (2002) 1147-1150.

[11] J.W. Stouwdam, G.A. Hebbink, J. Huskens, F.C.J.M. van Veggel, Chem. Mater. 15 (2003) 4604-4616.

[12] H.K. Jung, J.S. Oh, S.I. Seok, T.H. Lee, J. Lumin. 114 (2005) 307-313.

[13] B.Y. Ahn, S.I. Seok, S.I. Hong, J.S. Oh, H.K. Jung, W.J. Chung, Opt. Mater. 28 (2006) 374-379.

[14] J.S. Oh, S.I. Seok, H.K. Jung, Diffus. Defect Data, Pt. B 124-126 (2007) 471-474.

[15] H.Y. Gan, L. Li, C.T. DeRose, R.A. Norwood, C.R. De Silva, Z.P. Zheng, N. Peyghambarian, in: S. Jiang, M.J.F. Digonnet (Eds.), Conference on Optical Components and Materials IV, San Jose, CA (USA), Proceedings of the Society of Photo-Optical Instrumentation Engineers (SPIE), (2007) pp. 64690B-1-8.

[16] M.A. Lim, S.I. Seok, W.J. Chung, S.I. Hong, Opt. Mater. 31 (2008) 201-205.

[17] R. Lisiecki, W. Ryba-Romanowski, A. Speghini, M. Bettinelli, J. Lumin. 129 (2009) 521-525.

[18] E. López-Navarrete, M. Ocaña, J. Eur. Ceram. Soc. 22 (2002) 353-359.

[19] E. López-Navarrete, V.M. Orera, F.J. Lázaro, J.B. Carda, M. Ocaña, J. Am. Ceram. Soc. 87 (2004) 2108-2113.

[20] I.W. Lenggoro, B. Xia, H. Mizushima, K. Okuyama, N. Kijima, Mater. Lett. 50 (2001) 92-96.

[21] Y.C. Kang, E.J. Kim, D.Y. Lee, H.D. Park, J. Alloys Compd. 347 (2002) 266-270.

[22] Y.X. Ni, J.M. Hughes, A.N. Mariano, Am. Mineral. 80 (1995) 21-26.

[23] P. Yang, Z. Quan, C. Li, Z. Hou, W. Wang, J. Lin, J. Solid State Chem. 182 (2009) 1045-1054.

[24] K. Nakamoto, Infrared and Raman Spectra of Inorganic and Coordination Compounds, fourth ed., John Wiley & Sons, New York, 1986.

[25] R.D. Shannon, Acta Crystallogr., Sect. A: Found. Crystallogr. 32 (1976) 751-767.

[26] B.T. Stone, K.L. Bray, J. Non-cryst. Solids 197 (1996) 136-144.

[27] R.M. Almeida, X.M. Du, D. Barbier, X. Orignac, J. Sol-Gel Sci. Technol. 14 (1999) 209-216.

[28] L. Zhang, H. Hu, J. Phys. Chem. Solids 63 (2002) 575-579.

[29] G. De, W. Qin, J. Zhang, J. Zhang, Y. Wang, C. Cao, Y. Cui, Solid State Commun. 137 (2006) 483-487.

[30] C.C. Santos, I. Guedes, C.K. Loong, L.A. Boatner, A.L. Moura, M.T. de Araujo, C. Jacinto, M.V.D. Vermelho, J. Phys. D: Appl. Phys. 43 (2010) 025102-1-8.

[31] K. Byrappa, M.K. Devaraju, J.R. Paramesh, B. Basavalingu, K. Soga, J. Mater. Sci. 43 (2008) 2229-2233.

[32] J.W. Stouwdam, F.C.J.M. van Veggel, Nano Lett. 2 (2002) 733-737.

[33] H.T. Wong, H.L.W. Chan, J.H. Hao, Appl. Phys. Lett. 95 (2009) 022512-1-3.

[34] M. Ocaña, E. Cantelar, F. Cussó, Mater. Chem. Phys. 125 (2011) 224-230.

[35] J. Sun, X. Zhang, Z. Xia, H. Du, J. Appl. Phys. 111 (2012) 013101-1-7.

[36] M. Zhao, G. Li, J. Zheng, L. Li, L. Yang, CrystEngComm. 14 (2012) 2062-2070.

[37] M.D. Shinn, W.A. Sibley, M.G. Drexhage, R.N. Brown, Phys. Rev. B: Condens. Matter Mater. Phys. 27 (1983) 6635-6648.

[38] M. Pollnau, E. Heumann, T. Danger, G. Huber, Opt. Commun. 118 (1995) 250-254.

[39] J.A. Muñoz, B. Herreros, G. Lifante, F. Cusso, Phys. Status Solidi A 168 (1998) 525-530.

[40] R.S. Quimby, B.G. Aitken, J. Non-Cryst. Solids 320 (2003) 100-112.

[41] S. Xu, Z. Yang, G. Wang, S. Dai, J. Zhang, L. Hu, Z. Jiang, J. Alloys Compd. 377 (2004) 253-258.

[42] H. Lin, S. Tanabe, L. Lin, Y.Y. Hou, K. Liu, D.L. Yang, T.C. Ma, J.Y. Yu, E.Y.B. Pun, J. Lumin. 124 (2007) 167-172.

[43] H. Yang, Z. Dai, Z. Sun, J. Lumin. 124 (2007) 207-212.

[44] L.A. Riseberg, H.W. Moos, Phys. Rev. 174 (1968) 429-438.

[45] T. Miyakawa, D.L. Dexter, Phys. Rev. B: Condens. Matter Mater. Phys. 1 (1970) 2961-2969.

[46] C. B. Layne, W. H. Lowdermilk, M. J. Weber, Phys. Rev. B: Condens. Matter Mater. Phys. 16 (1977) 10-20.

[47] R. Reisfeld, Y. Eckstein, J. Chem. Phys. 63 (1975) 4001-4012.

[48] J.M.F. van Dijk, M.F.H. Schuurmans, J. Chem. Phys. 78 (1983) 5317-5323.

[49] M.F.H. Schuurmans, J.M.F. van Dijk, Physica B 123 (1984) 131-155.

[50] K. Amezawa, H. Maekawa, Y. Tomii, N. Yamamoto, Solid State Ionics 145 (2001) 233-240.

[51] B.T. Stone, K.L. Bray, J. Non-Cryst. Solids 197 (1996) 136-144.

[52] C. Stronhöfer, J. Fock, H.C. Vasconcelos, R.M. Almeida, J. Non-Cryst. Solids (1998) 182-191.

[53] R.M. Almeida, X.M. Du, D. Barbier, X. Orignac, J. Sol-Gel Sci. Technol. 14 (1999) 209-216.

[54] P. Etienne, P. Coudray, J. Porque, Y. Moreau, Opt. Commun. 174 (2000) 413-418.

[55] L. Zhang, H. Hu, J. Phys. Chem. Solids 63 (2002) 575-579

[56] J. Oliva, O. Meza, L.A. Diaz-Torres, P. Salas, E. del la Rosa, A. Martinez, C. Angeles-Chavez, J. Opt. Soc. Am. B 28 (2011) 649-657

Table 1. Crystallite size of the $LaPO_4$:Er sample as prepared and after heating at different temperatures

Temperature (ºC)	**Crystal size (nm)**	**Technique**
As prepared	12	XRD
600	15	XRD
700	18	XRD
800	37	XRD
900	50	XRD
950	50-150	SEM

Table 2. Unit cell parameters measured for the $LaPO_4$:Er sample heated at 950 ºC and for an undoped $LaPO_4$ sample prepared under similar conditions.

	a/Å	**b/Å**	**c/Å**	**V/Å ^{3}**
$LaPO_4$	6.5126(2)	7.0762(2)	8.2913(3)	306.84670
$Er_{0.02}La_{0.98}PO_4$	6.5069(1)	7.0683(1)	8.2813(2)	305.8756

Table 3. Fitting parameters of the 1.5 μm luminescence decay of Er^{3+} ions in $LaPO_4$, using a double exponential dependence (eq. (1)). The luminescent quantum yield ($\langle\eta\rangle = \langle\tau\rangle/\tau_{rad}$) is calculated using the average experimental decay time (eq. (2)) and the radiative decay time reported in [17]

Calcination Temperature (ºC)	**A_S**	**τ_S (ms)**	**A_L**	**τ_L (ms)**	**$\langle\tau\rangle$ (ms)**	**$\langle\eta\rangle$ (%)**
As prepared	0.42	0.16	0.58	0.85	0.76	11
600	0.35	0.49	0.65	1.74	1.57	23
700	0.40	0.67	0.60	2.26	2.00	30
800	0.17	1.24	0.83	4.42	4.25	63
900	0.24	1.91	0.76	5.98	5.60	84
950	0.17	1.53	0.83	6.70	6.47	96

FIGURE CAPTIONS

Fig. 1.- SEM micrographs for the $LaPO_4$:Er sample as prepared and after heating at 950ºC.

Fig. 2.- XRD pattern obtained for the $LaPO_4$:Er sample as prepared and after heating at different temperatures

Fig. 3.- FTIR spectra obtained for the $LaPO_4$:Er sample as prepared and after heating at different temperatures

Fig. 4.- TGA curve obtained for the $LaPO_4$:Er sample.

Fig. 5.- Absorption spectrum of Er^{3+} ions in $LaPO_4$ microspheres. The absorption bands are labeled indicating the absorbing multiplet from the $^4I_{15/2}$ ground state.

Fig. 6.- Near infrared luminescence spectra of Er^{3+}-doped $LaPO_4$ microspheres after different calcination temperatures. The inset shows a partial energy level diagram indicating the main optical transitions involved in the photoluminescence process.

Fig. 7.- Luminescence decays of the 1.5 μm emission of Er^{3+}-ions in $LaPO_4$ microspheres subjected to different calcination temperatures. The lines correspond to the least-squares fitting using a bi-exponential decay (eq. (1)), with the parameters summarized in Table 3.

Fig. 8.- Luminescence quantum yield (circles), calculated as $\langle\eta\rangle = \langle\tau\rangle/\tau_{rad}$, as function of the calcination temperature. The line has been drawn to guide the eye.

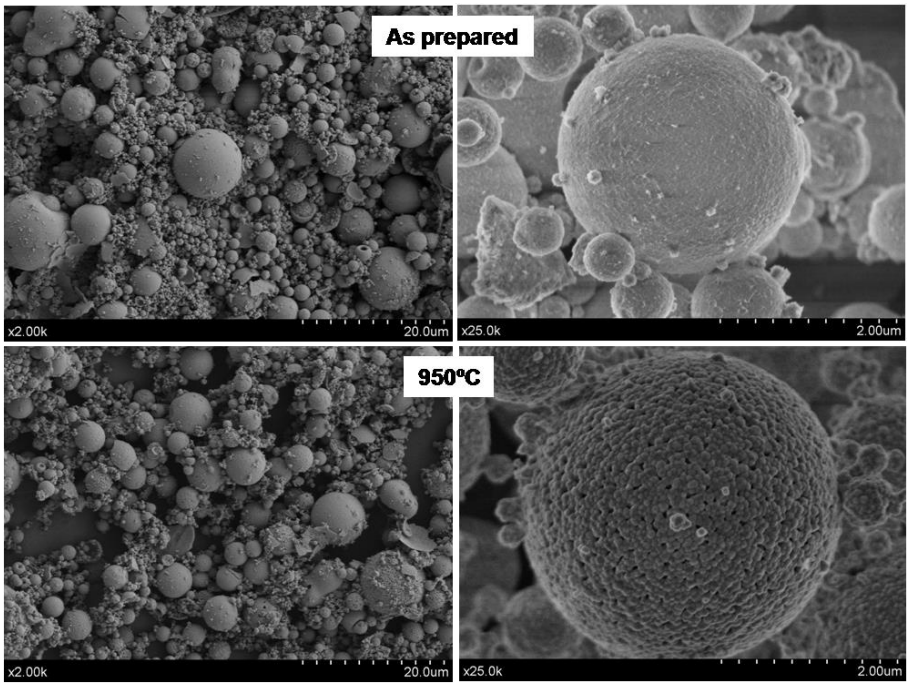
As prepared
x2.00k
20.0um
x25.0k
2.00um
950°C
x2.00k
20.0um
x25.0k
2.00um

Fig. 1

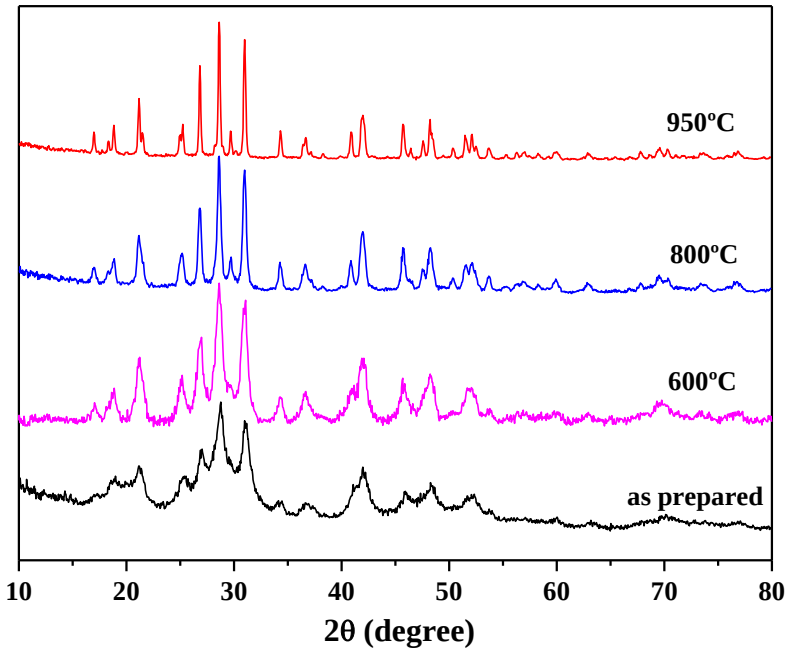

Fig. 2

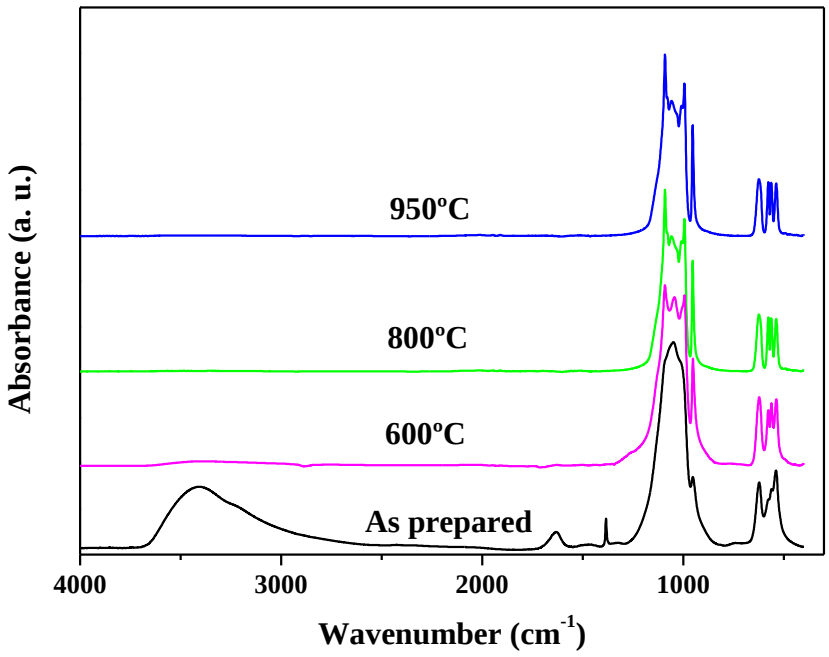
950ºC
800ºC
600ºC
As prepared
Absorbance (a. u.)
4000
3000
2000
1000
Wavenumber (cm-1)

Fig. 3

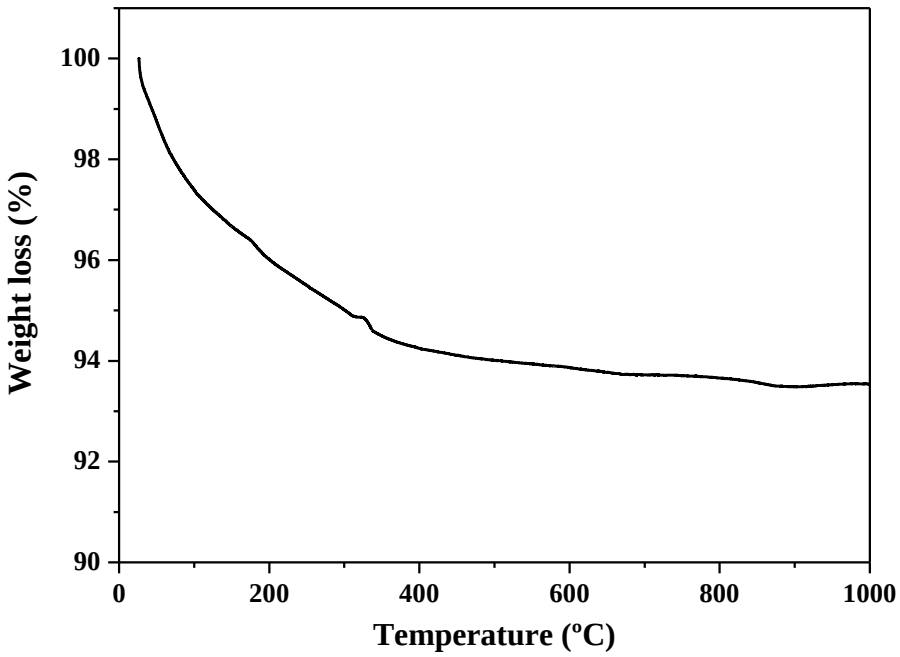
Weight loss (%)
100
98
96
94
92
90
0
200
400
600
800
1000
Temperature (°C)

Fig. 4

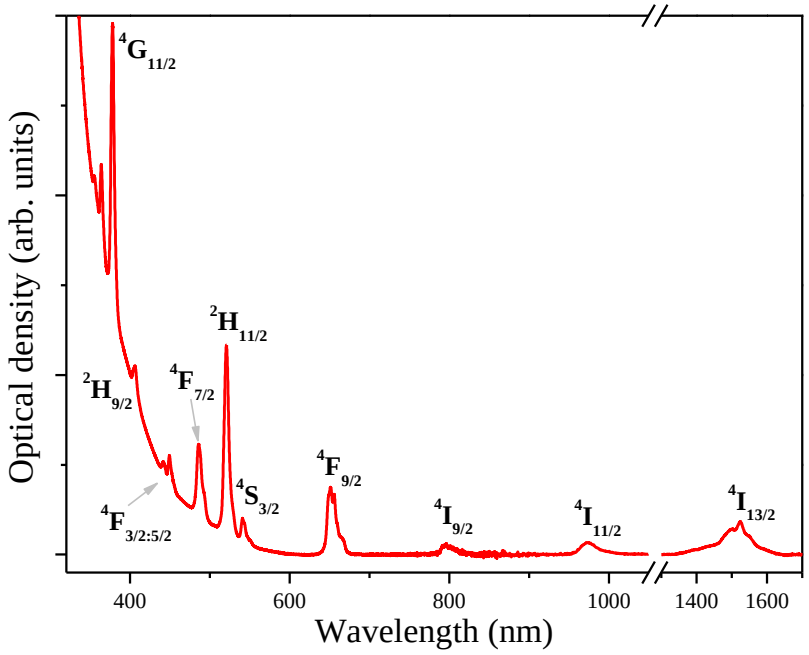
Optical density (arb. units)
Wavelength (nm)
400
600
800
1000
1400
1600
$^4G_{11/2}$
$^2H_{11/2}$
$^2H_{9/2}$
$^4F_{7/2}$
$^4S_{3/2}$
$^4F_{9/2}$
$^4F_{3/2:5/2}$
$^4I_{9/2}$
$^4I_{11/2}$
$^4I_{13/2}$

Fig. 5

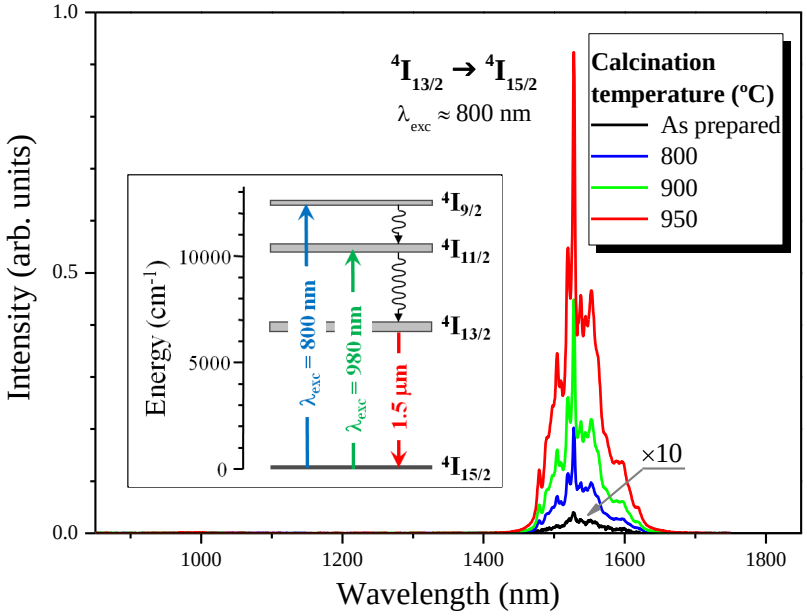
1.0
0.5
0.0
Intensity (arb. units)
1000
1200
1400
1600
1800
Wavelength (nm)
$^4I_{13/2} \rightarrow {}^4I_{15/2}$
$\lambda_{exc} \approx 800$ nm
Calcination temperature (°C)
As prepared
800
900
950
×10
Energy (cm^{-1})
10000
5000
0
$^4I_{9/2}$
$^4I_{11/2}$
$^4I_{13/2}$
$^4I_{15/2}$
λ_{exc} = 800 nm
λ_{exc} = 980 nm
1.5 μm

Fig. 6

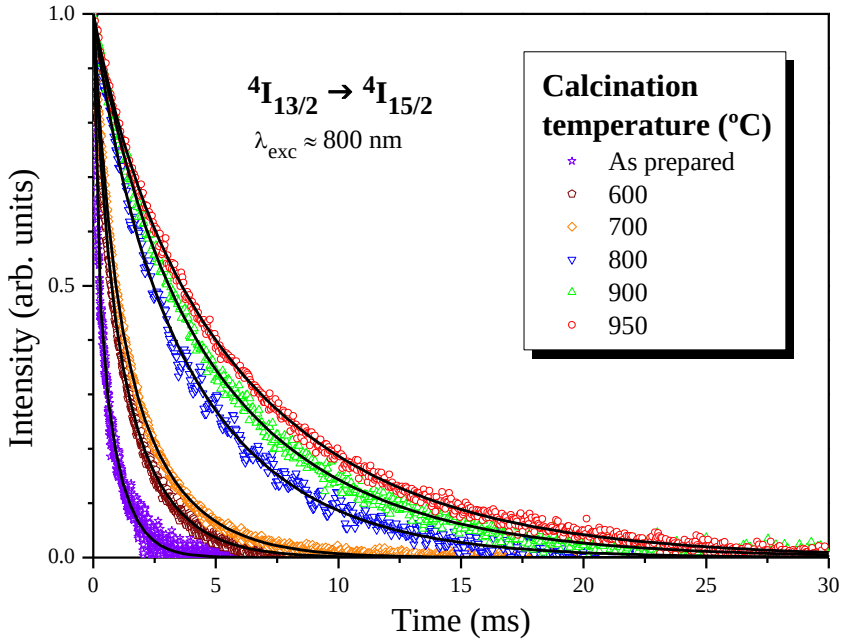
1.0
0.5
0.0
Intensity (arb. units)
0
5
10
15
20
25
30
Time (ms)
$^4I_{13/2} \rightarrow {}^4I_{15/2}$
$\lambda_{exc} \approx 800$ nm
Calcination temperature (°C)
As prepared
600
700
800
900
950

Fig. 7

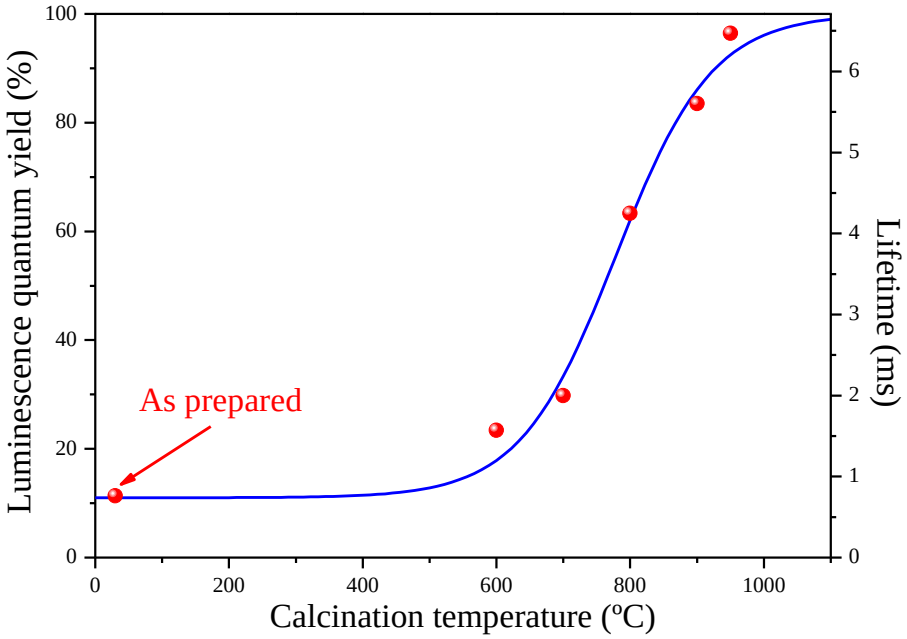
Luminescence quantum yield (%)
Lifetime (ms)
Calcination temperature (ºC)
As prepared
0
20
40
60
80
100
0
1
2
3
4
5
6
0
200
400
600
800
1000

Fig. 8